Electronic Supplementary Material (ESI) for ChemComm.

Supporting Information

I. Materials and Methods

All manipulations were carried out using break-and-seal and glove-box techniques under an atmosphere of argon.[1] Tetrahydrofuran (THF) and hexanes (Sigma Aldrich) were dried over Na/benzophenone and distilled prior to use. Tetrahydrofuran-d_8 (≥99.5 atom %D, Sigma Aldrich) was dried over NaK_2 alloy and vacuum-transferred. Lithium (99 %), sodium (99.9 %), 18-crown-6 ether (99 %), and [2.2.2]cryptand (98 %) were purchased from Sigma Aldrich and used as received. $C_{72}H_{48}$ (**1**) was prepared and purified according to the previously reported procedure.[2] The UV-Vis spectra were recorded on a Thermo Scientific Evolution 201 UV-Visible Spectrophotometer. The ^{1}H, ^{7}Li, ^{13}C and ^{1}H-^{1}H COSY NMR spectra were recorded on a Bruker Ascend-500 spectrometer (500 MHz for ^{1}H, 194 MHz for ^{7}Li, and 126 MHz for ^{13}C). Chemical shifts (δ) are reported in parts per million (ppm) and referenced to the resonances of the corresponding solvent used. The low-temperature NMR experiment was controlled by a Cryo Diffusion cryogenic tank probe, and liquid N_2 was used as a cooling source. Mass spectra were acquired using a DART-SVP ion source (IonSense, Saugus, MA, USA) coupled to a JEOL AccuTOF time-offlight mass spectrometer (JEOL USA, Peabody, MA, USA); settings: DART positive mode, 5–20 V (orifice voltage), 500 °C (heater temperature). The presence of the interstitial THF molecules coupled with extreme air- and moisture sensitivity of the crystals prevented obtaining elemental analysis data.

[{Li$^+$([2.2.2]cryptand}$_2$(**1**$_{TR}^{2-}$)]·2THF (**2**·2THF)

THF (1.5 mL) was added to a customized glass system containing excess Li (5.0 mg, 0.710 mmol), **1** (1.5 mg, 0.002 mmol), and [2.2.2]cryptand (3.0 mg, 0.008 mmol). The mixture was allowed to stir under argon at 25 °C for 30 minutes in a closed system. The initial off-white color of the suspension (neutral ligand) has changed to pale blue after 15 minutes, deepened to dark purple after 20 minutes and remained the same color until the reaction was stopped. The suspension was filtered, and the purple filtrate was layered with 1.2 mL of hexanes. The ampule was sealed and stored at 5 °C. After 5 days, some black plates were present in moderate yield. Yield: 1.2 mg, 40%. UV-Vis (THF, λ_{max}, nm): 486, 572. ^{1}H NMR (THF-d_8, 25 °C, δ, ppm): 2.48–3.48 (36H, [2.2.2]cryptand), 4.93–4.94 (2H, **1**$_{TR}^{2-}$), 5.91–5.99 (4H, **1**$_{TR}^{2-}$), 6.16–6.26 (12H, **1**$_{TR}^{2-}$), 6.35–6.45 (10H, **1**$_{TR}^{2-}$), 6.68–6.70 (4H, **1**$_{TR}^{2-}$), 6.93–7.00 (8H, **1**$_{TR}^{2-}$), 7.05–7.08 (2H, **1**$_{TR}^{2-}$), 7.11–7.13 (2H, **1**$_{TR}^{2-}$), 7.21–7.22 (2H, **1**$_{TR}^{2-}$), 8.06–8.08 (2H, **1**$_{TR}^{2-}$).

[{Na^+(18-crown-6)$(THF)_2$}$_2$($\mathbf{1}_{TR}^{2-}$)]·3THF (3·3THF)

THF (1.5 mL) was added to a customized glass system containing excess Na (2.0 mg, 0.087 mmol), **1** (2.0 mg, 0.002 mmol), and 18-crown-6 ether (1.5 mg, 0.006 mmol). The mixture was allowed to stir under argon at 25 °C for 30 minutes in a closed system. The initial off-white color of the suspension (neutral ligand) has changed to pale blue after 10 minutes, deepened to dark purple after 15 minutes and remained the same until the reaction was stopped. The suspension was filtered, and the purple filtrate was layered with 1.2 mL of hexanes. The ampule was sealed and stored at 5 °C. Dark plate-shaped crystals were present in good yield after 10 days. Yield: 3.1 mg, 80%. UV-Vis (THF, λ_{max}, nm): 479, 580. ^{1}H NMR (THF-d_8, 25 °C, δ, ppm): 3.51 (48H, 18-crown-6), 4.92–4.93 (2H, $\mathbf{1}_{TR}^{2-}$), 5.89–5.95 (4H, $\mathbf{1}_{TR}^{2-}$), 6.15–6.25 (12H, $\mathbf{1}_{TR}^{2-}$), 6.35–6.44 (10H, $\mathbf{1}_{TR}^{2-}$), 6.68–6.70 (4H, $\mathbf{1}_{TR}^{2-}$), 6.90–7.06 (10H, $\mathbf{1}_{TR}^{2-}$), 7.10–7.12 (2H, $\mathbf{1}_{TR}^{2-}$), 7.19–7.20 (2H, $\mathbf{1}_{TR}^{2-}$), 8.03–8.05 (2H, $\mathbf{1}_{TR}^{2-}$).

II. UV-Vis Spectroscopic Investigation

Sample preparation: THF (2.0 mL) was added to an airtight storage ampule containing Na metal (0.50 mg, 0.022 mmol), [2.2.2]cryptand (0.20 mg, 7.6×10^{-4} mmol), and **1** (0.30 mg, 3.3×10^{-4} mmol); and UV-Vis spectra were monitored at different reaction times (total 20 hours) at room temperature.

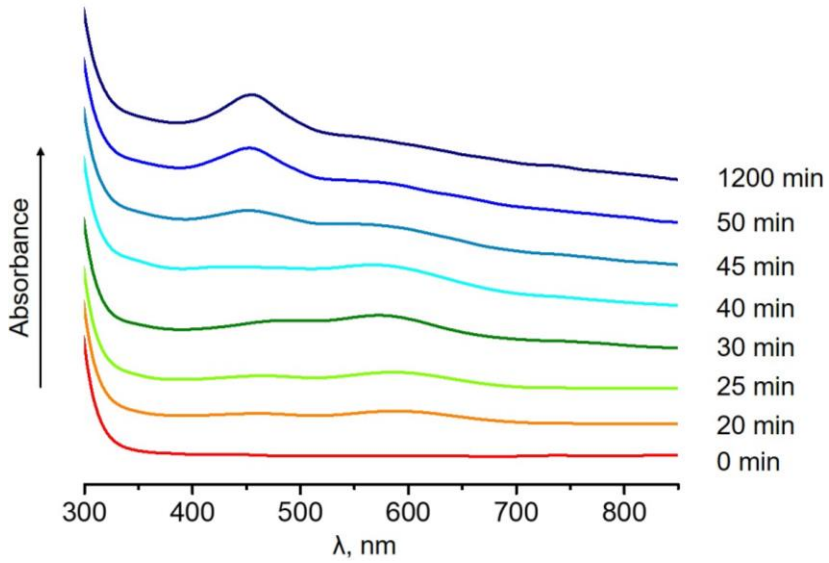

Fig. S1 UV-Vis spectra of Li/[2.2.2]cryptand/**1** in THF.

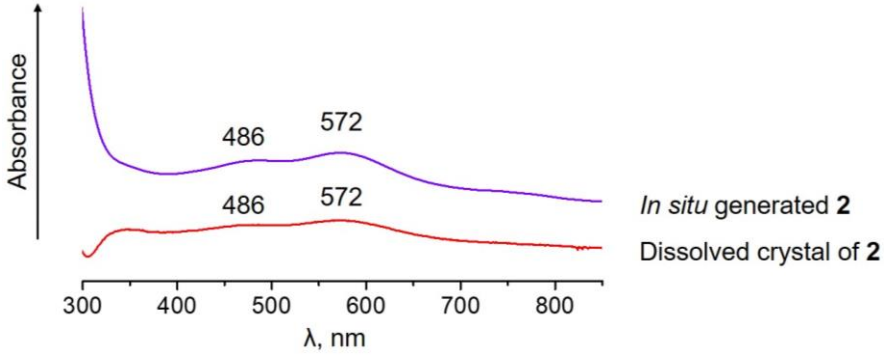

Fig. S2 UV-Vis spectra of i*n situ* generated **2** and crystals of **2** dissolved in THF.

Sample preparation: THF (2.0 mL) was added to an airtight storage ampule containing Na metal (0.50 mg, 0.022 mmol), 18-crown-6 (0.20 mg, 7.6×10^{-4} mmol), and **1** (0.30 mg, 3.3×10^{-4} mmol); and UV-Vis spectra were monitored at different reaction times (total 24 hours) at room temperature.

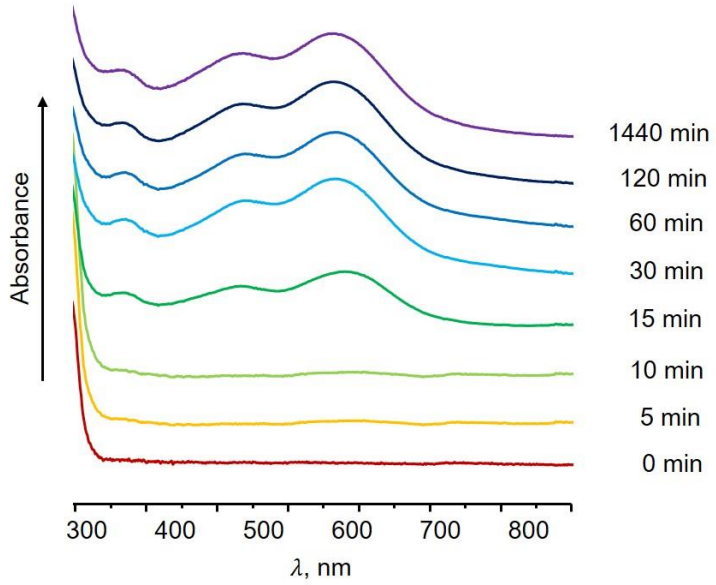

Fig. S3 UV-Vis spectra of Na/18-crown-6/**1** in THF.

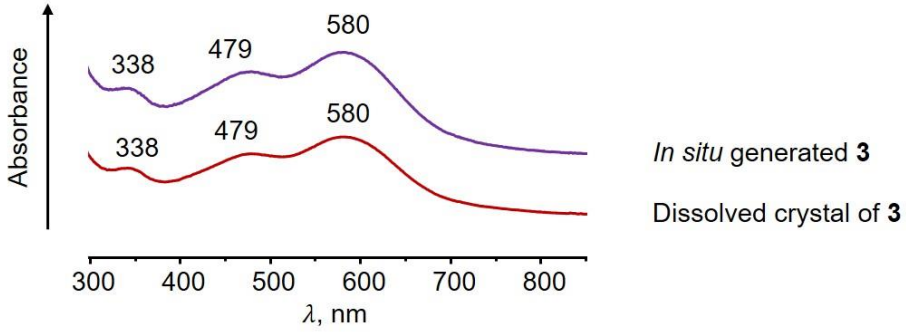

Fig. S4 UV-Vis spectra of i*n situ* generated **3** and crystals of **3** dissolved in THF.

III. NMR Spectroscopic Investigation

Sample preparation: Crystals of **2** or **3** (3.0 mg) were washed several times with hexanes, dried *in-vacuo*, and dissolved in THF-d_8 (0.70 mL). The resulting solution was transferred to an NMR tube that was sealed under argon.

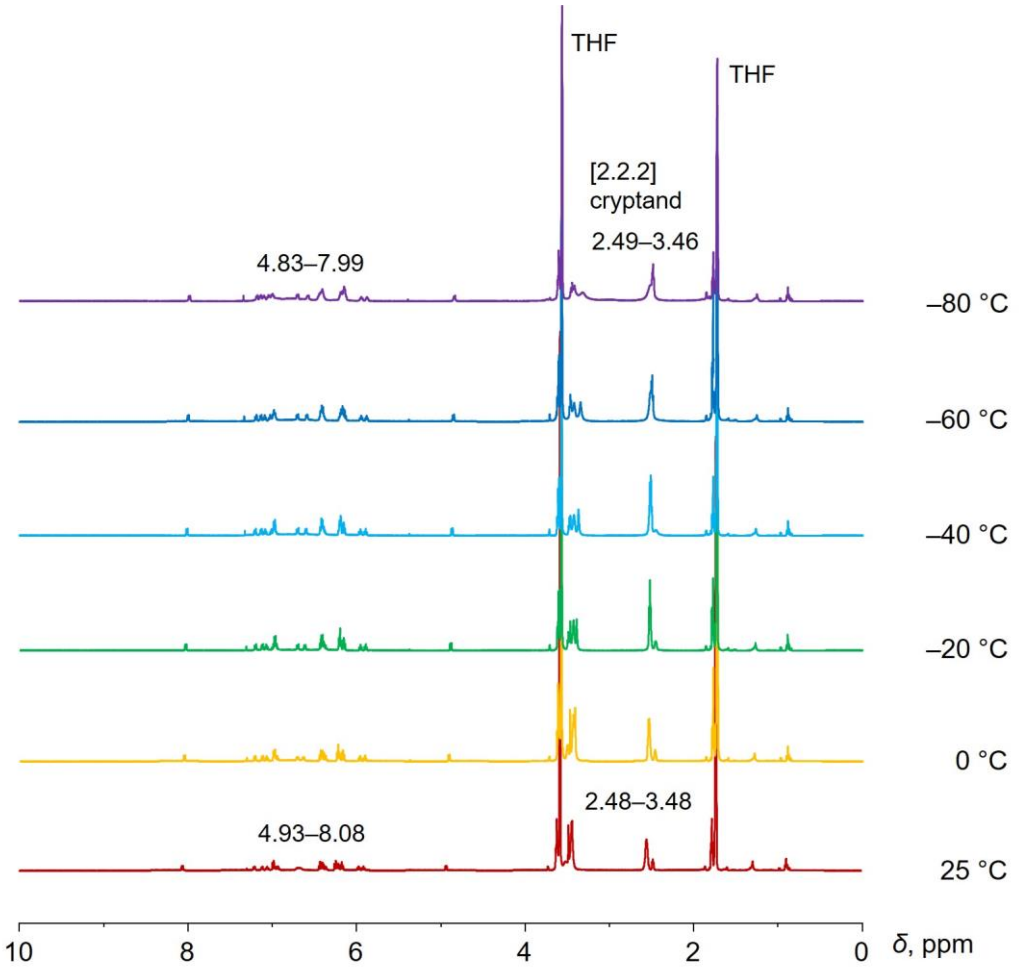

Fig. S5 Variable-temperature ^{1}H NMR spectra of **2** in THF-d_8.

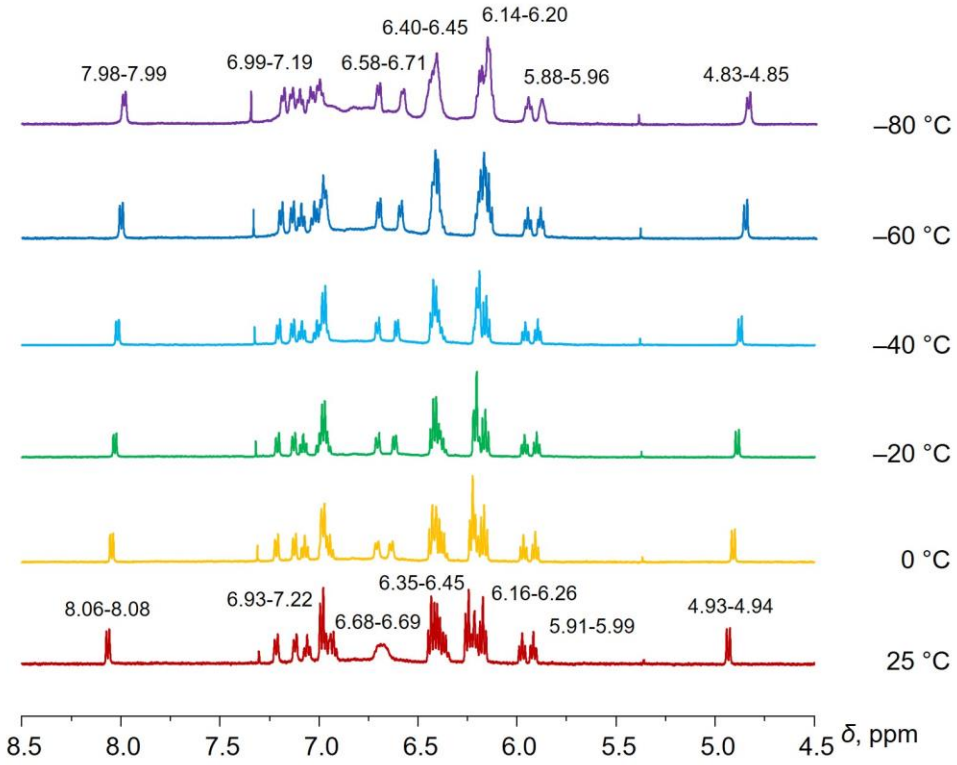

Fig. S6 Variable-temperature ^{1}H NMR spectra of **2** in THF-d_8 with chemical shifts at 25 ºC and –80 ºC, aromatic region.

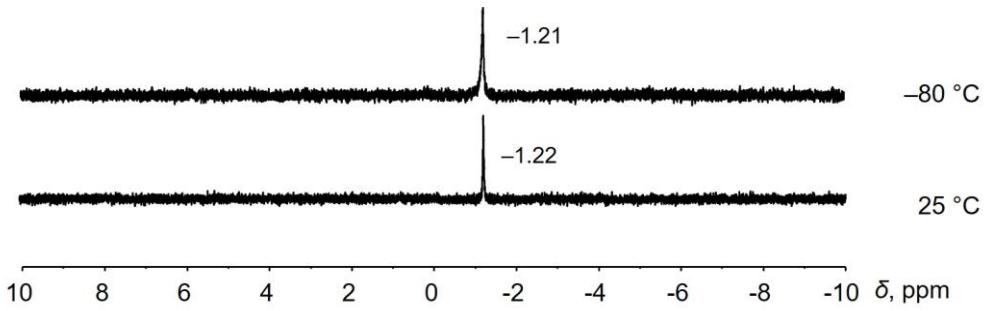

Fig. S7 ^{7}Li NMR spectra of **2** in THF-d_8 at 25 ºC and –80 ºC.

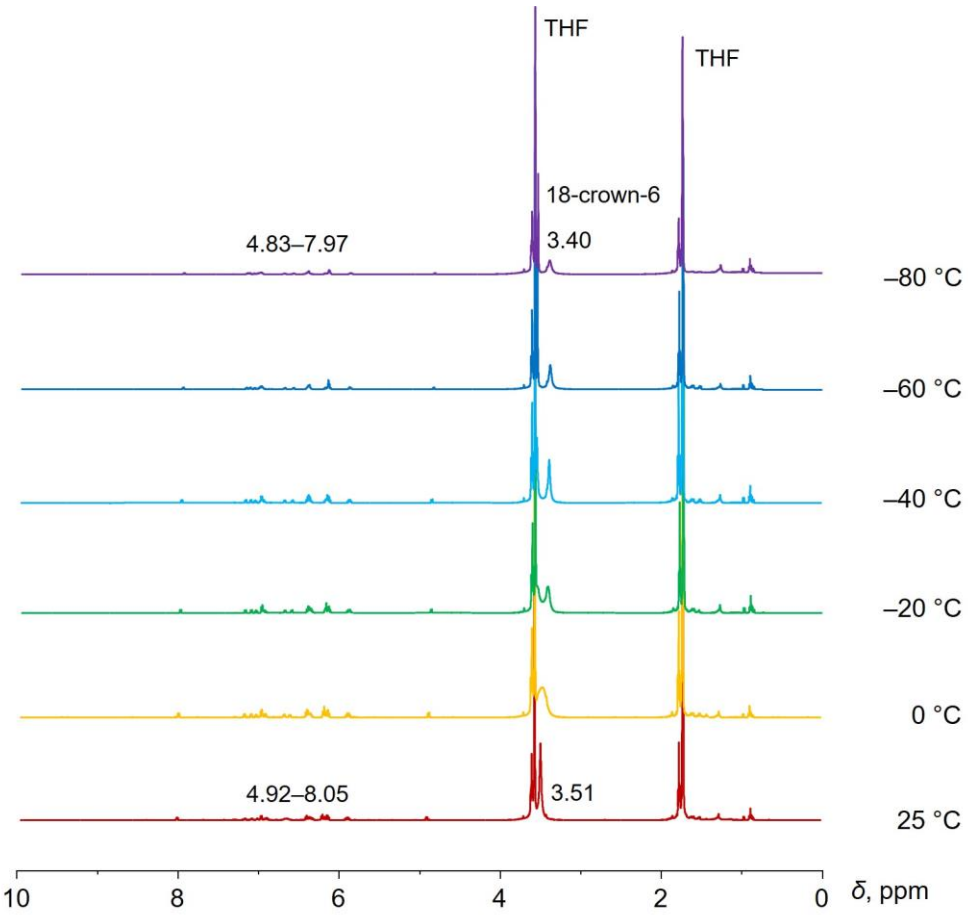

Fig. S8 Variable-temperature ^{1}H NMR spectra of **3** in THF-d_8.

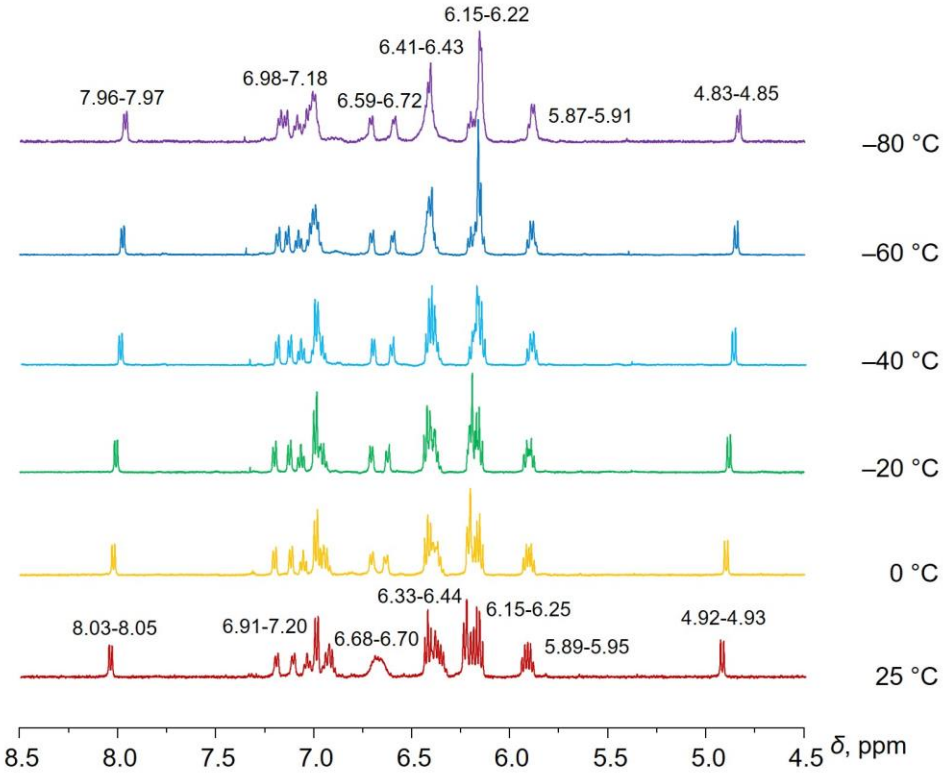

Fig. S9 Variable-temperature ^{1}H NMR spectra of **3** in THF-d_8 with chemical shifts at 25 ºC and –80 ºC, aromatic region.

Sample preparation: THF-d_8 (0.60 mL) was added to an NMR tube containing excess Li metal (2.0 mg, 0.290 mmol), [2.2.2]cryptand (4.0 mg, 0.011 mmol), and **1** (2.0 mg, 0.002 mmol). The NMR tube was sealed under argon. The initial color of the mixture was colorless. The mixture was allowed to sit for 30 min to afford a deep purple solution. The Li metal was decanted from the mixture, and the NMR spectra were collected.

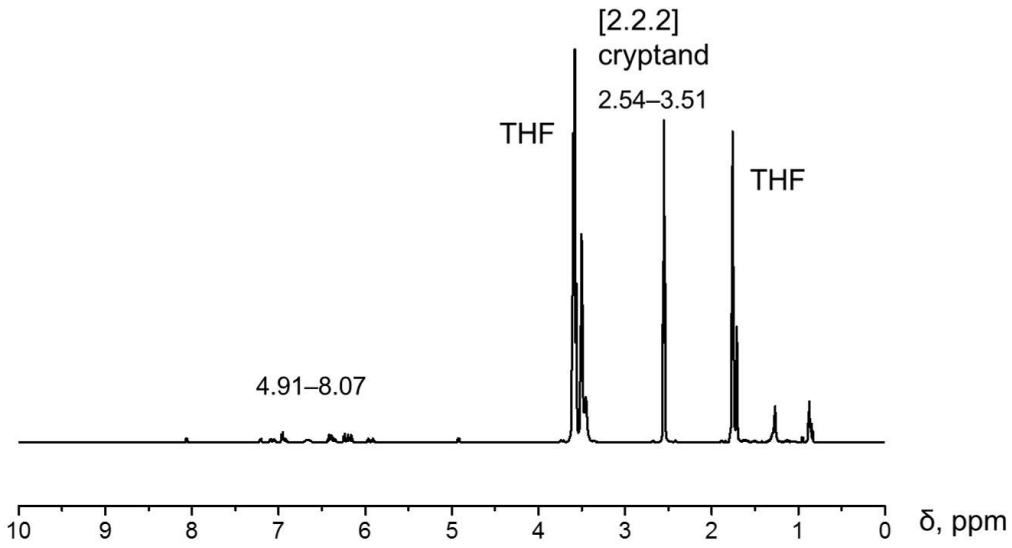

Fig. S10 ^{1}H NMR spectrum of *in situ* generated **2** in THF-d_8 at 25 ºC.

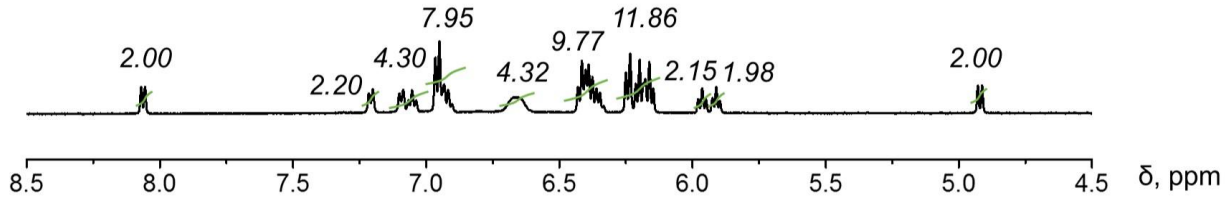

Fig. S11 ^{1}H NMR spectrum of *in situ* generated **2** in THF-d_8 at 25 ºC with integrations, aromatic region.

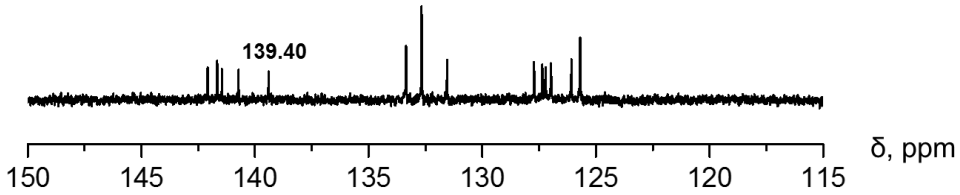

Fig. S12 ^{13}C NMR spectrum of **1** in THF-d_8 at 25 °C, aromatic region.

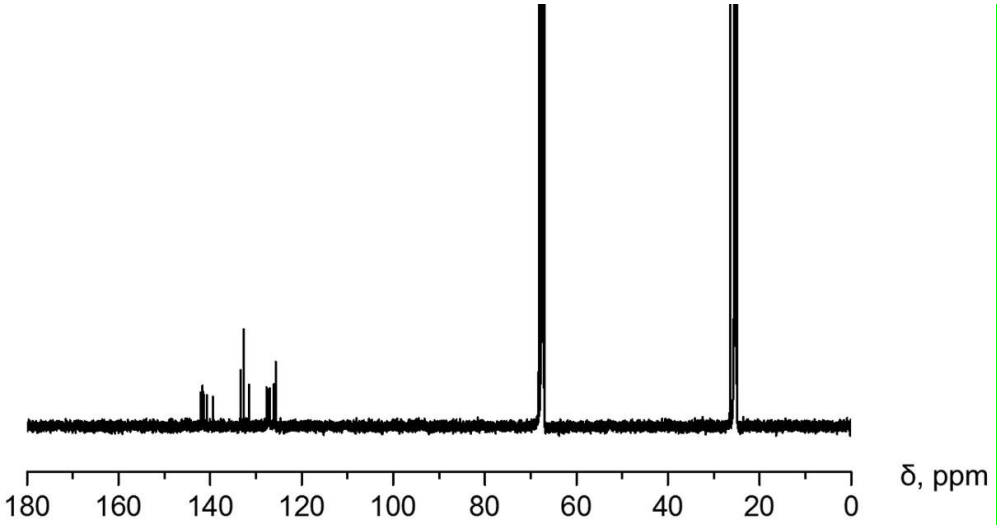

Fig. S13 ^{13}C NMR spectrum of **1** in THF-d_8 at 25 °C.

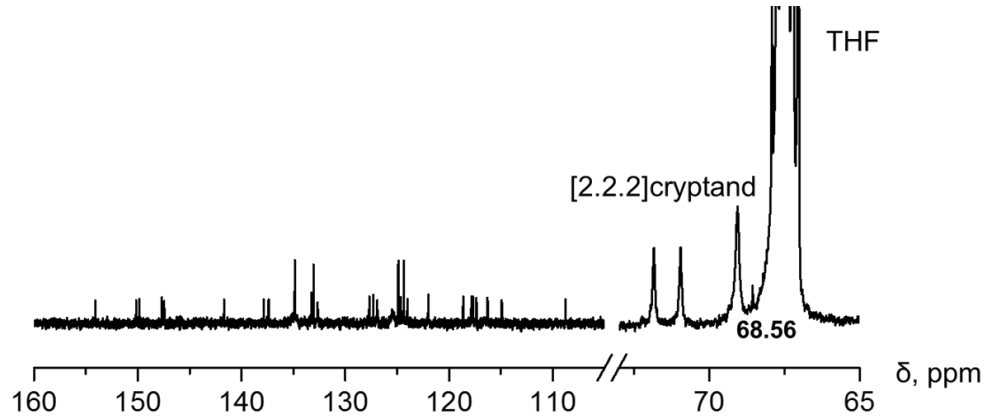

Fig. S14 ^{13}C NMR spectrum of *in situ* generated **2** in THF-d_8 at 25 °C, selected region.

Sample preparation: THF-d_8 (0.60 mL) was added to an NMR tube containing excess Na metal (2.0 mg, 0.087 mmol), 18-crown-6 (2.0 mg, 0.008 mmol), and **1** (3.0 mg, 0.003 mmol). The NMR tube was sealed under argon. The initial color of the mixture was colorless. The mixture was allowed to sit for 24 hours to afford a deep purple solution. The Na metal was decanted from the mixture and the NMR spectra were collected.

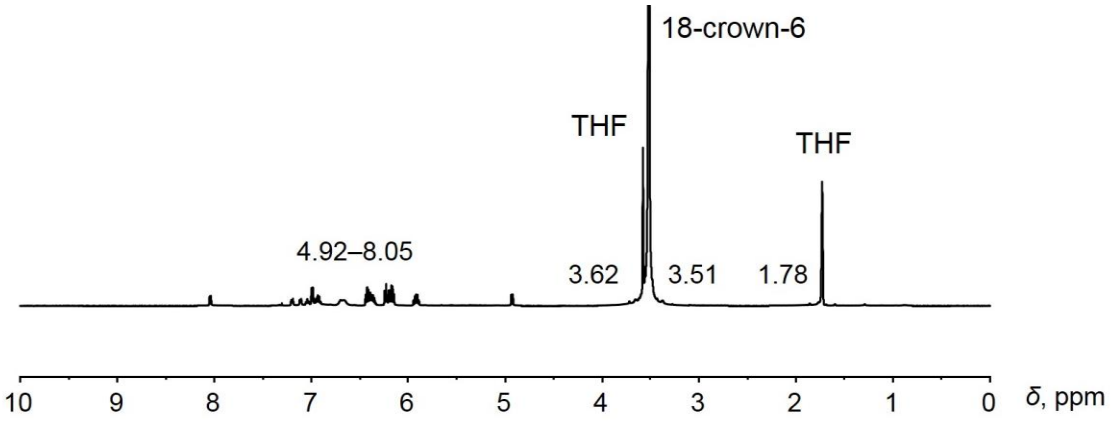

Fig. S15 ^{1}H NMR spectrum of *in situ* generated **3** in THF-d_8 at 25 ºC.

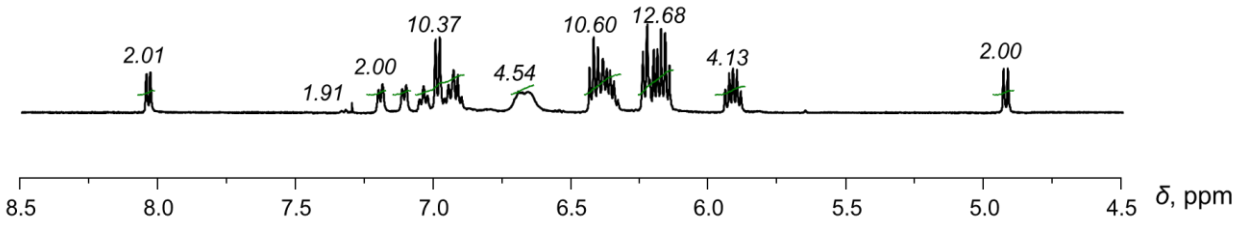

Fig. S16 ^{1}H NMR spectrum of *in situ* generated **3** in THF-d_8 at 25 ºC with integrations, aromatic region.

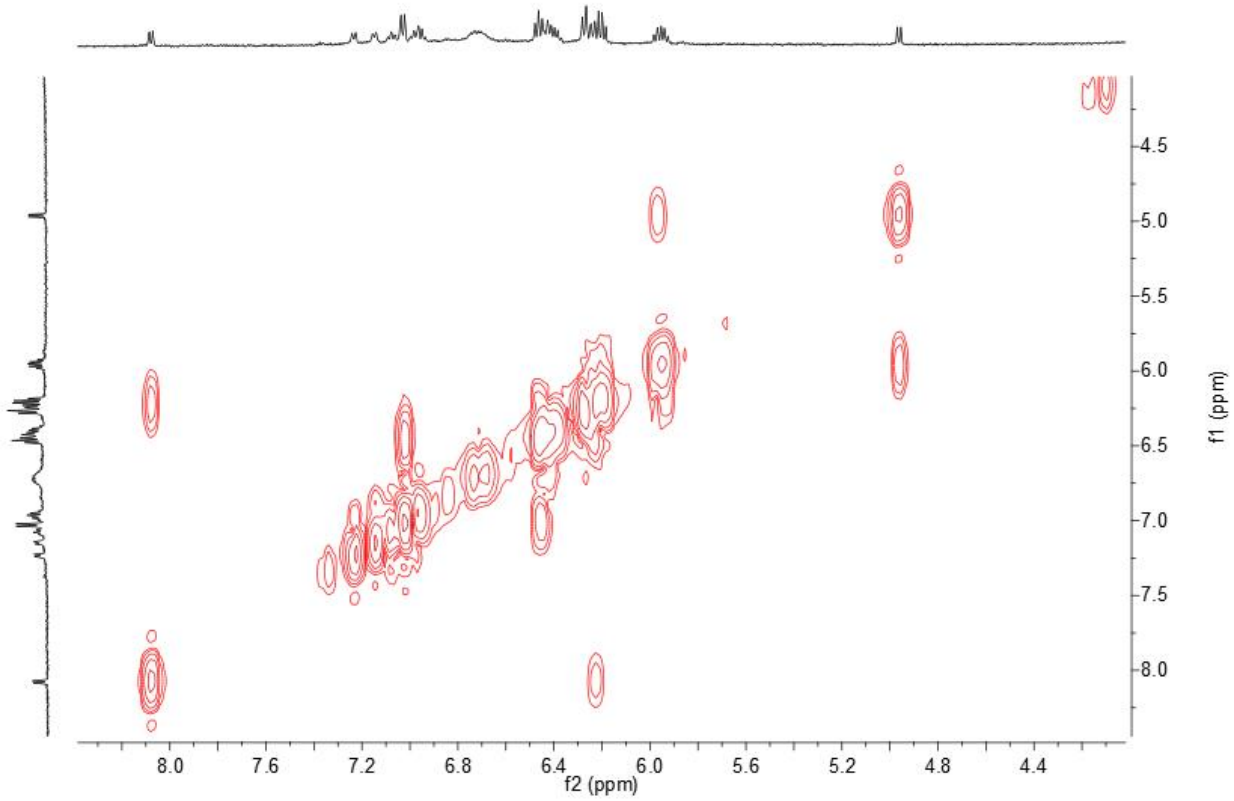

Fig. S17 ^{1}H-^{1}H COSY spectrum of *in situ* generated **3** in THF-d_8 at 25 °C, aromatic region.

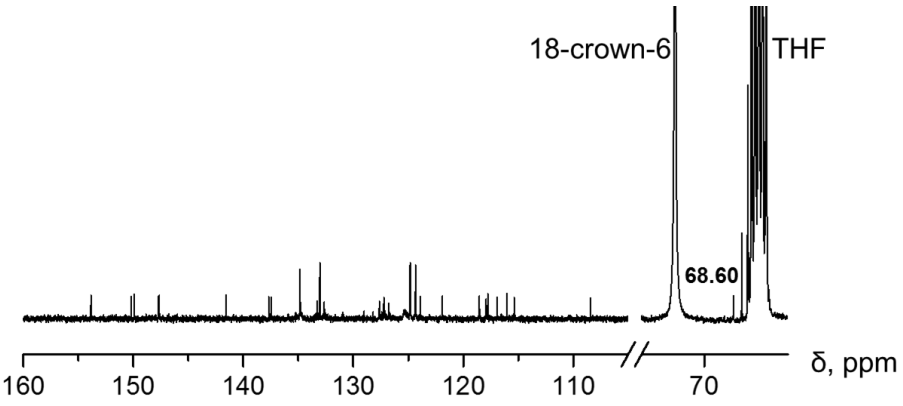

Fig. S18 ^{13}C NMR spectrum of *in situ* generated **3** in THF-d_8 at 25 °C, selected region.

IV. Study of Redox Reversibility

Sample preparation for NMR study: THF-d_8 (0.60 mL) was added to an NMR tube containing **1** (4.0 mg, 0.004 mmol), Li (2.0 mg, 0.286 mmol), and [2.2.2]cryptand (3.0 mg, 0.008 mmol). The tube was sealed under argon. The ^{1}H and ^{13}C NMR spectra of **1** were collected immediately, and that of *in situ* generated **2** were collected after 30 minutes. The solution was then exposed to air by opening the tube. The resulting off-white solution was checked as the spectra of a quenched product.

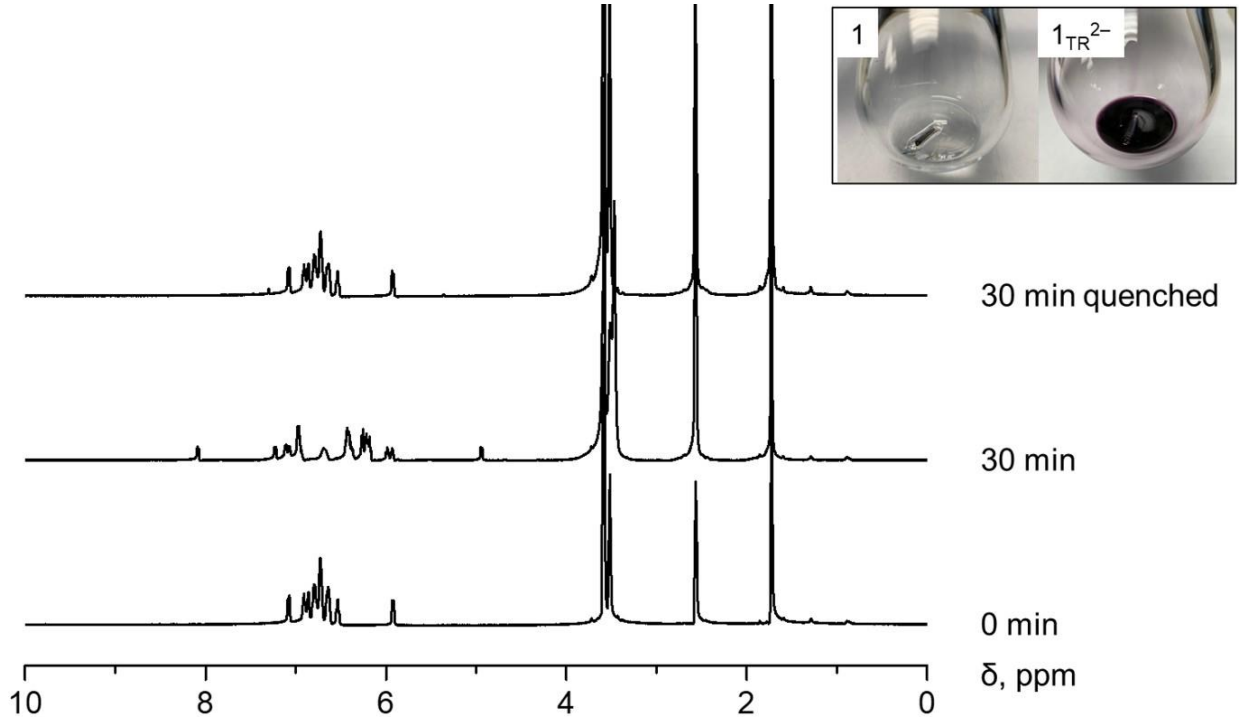

Fig. S19 ^{1}H NMR spectra of **1**, *in situ* generated $\mathbf{1}_{TR}^{2-}$ with Li and [2.2.2]cryptand, and its quenched product, 25 °C in THF-d_8.

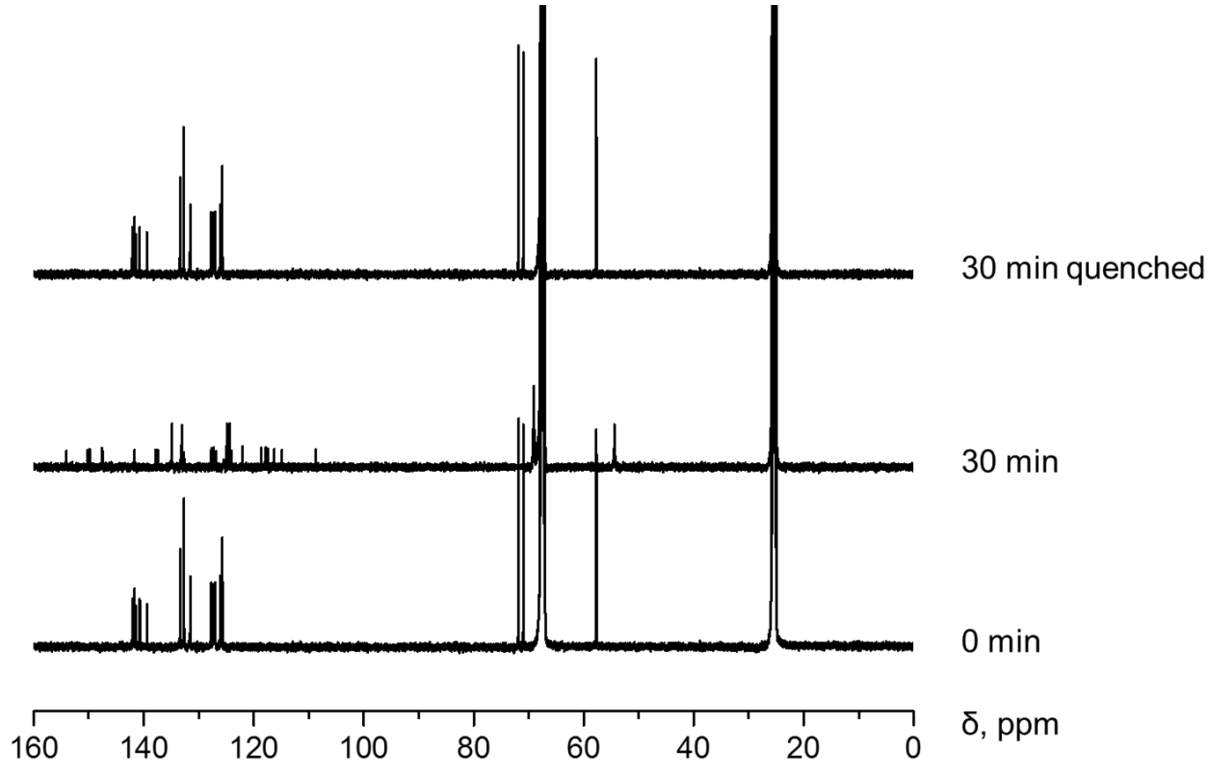

Fig. S20 ^{13}C NMR spectra of **1**, *in situ* generated $\mathbf{1}_{TR}^{2-}$ with Li and [2.2.2]cryptand, and its quenched product, 25 °C in THF-d_8.

Sample preparation for NMR study: THF-d_8 (0.80 mL) was added to an NMR tube containing **1** (4.0 mg, 0.004 mmol), Na (2.3 mg, 0.100 mmol), and 18-crown-6 ether (2.3 mg, 0.009 mmol). The tube was sealed under argon. The ^{1}H and ^{13}C NMR spectra of **1** were collected immediately, and that of *in situ* generated **3** were collected after 20 minutes. The solution was then exposed to air by opening the tube. The resulting off-white solution was checked as the spectra of a quenched product.

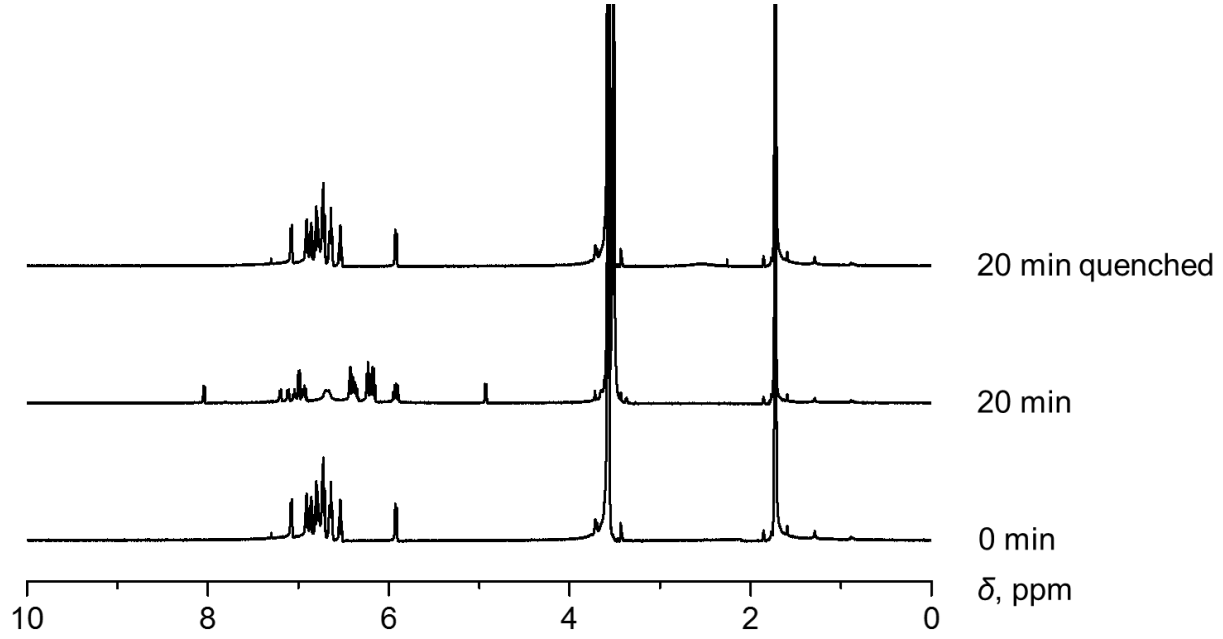

Fig. S21 ^{1}H NMR spectra of **1**, *in situ* generated $\mathbf{1}_{TR}^{2-}$ with Na and 18-crown-6 ether, and its quenched product, 25 °C in THF-d_8.

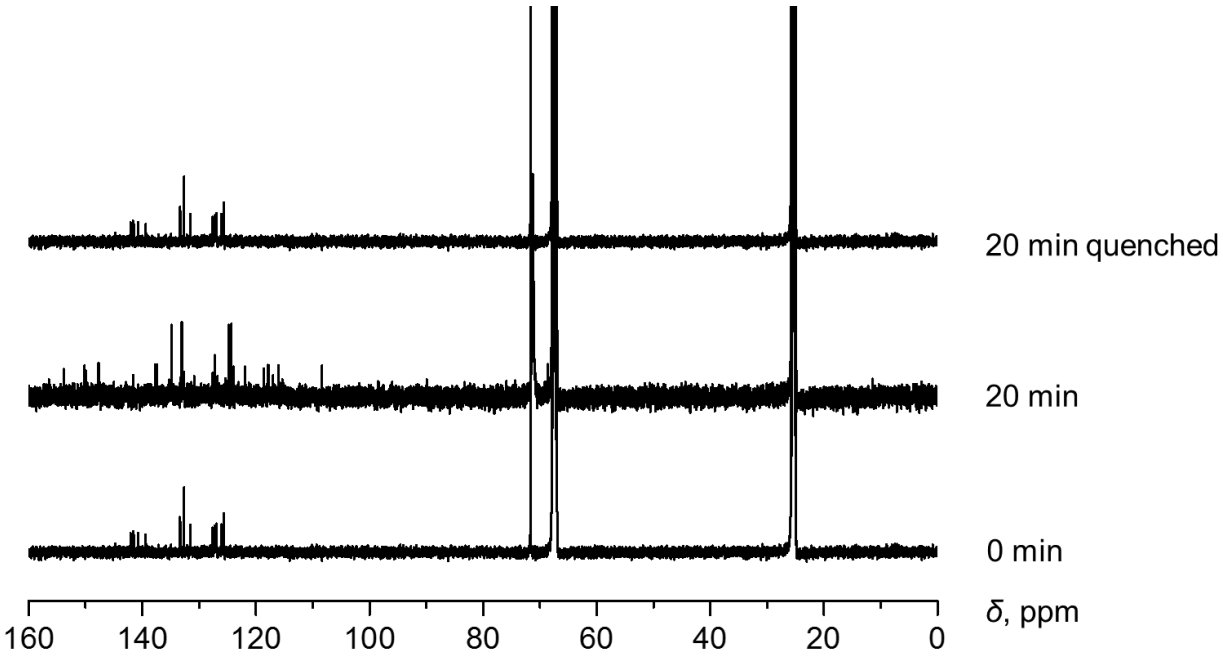

Fig. S22 ^{13}C NMR spectra of **1**, *in situ* generated $\mathbf{1}_{TR}^{2-}$ with Na and 18-crown-6 ether, and its quenched product; 25 °C in THF-d_8.

Sample preparation for DART-MS study: THF (2.0 mL) was added to a glass tube containing **1** (2.0 mg, 0.002 mmol), Na (2.0 mg, 0.087 mmol), and 18-crown-6 (1.2 mg, 0.005 mmol). The tube was sealed under argon. After 48 hours, the solution was exposed to air by opening the tube, and the spectrum was recorded as quenched product of $\mathbf{1}_{TR}^{2-}$.

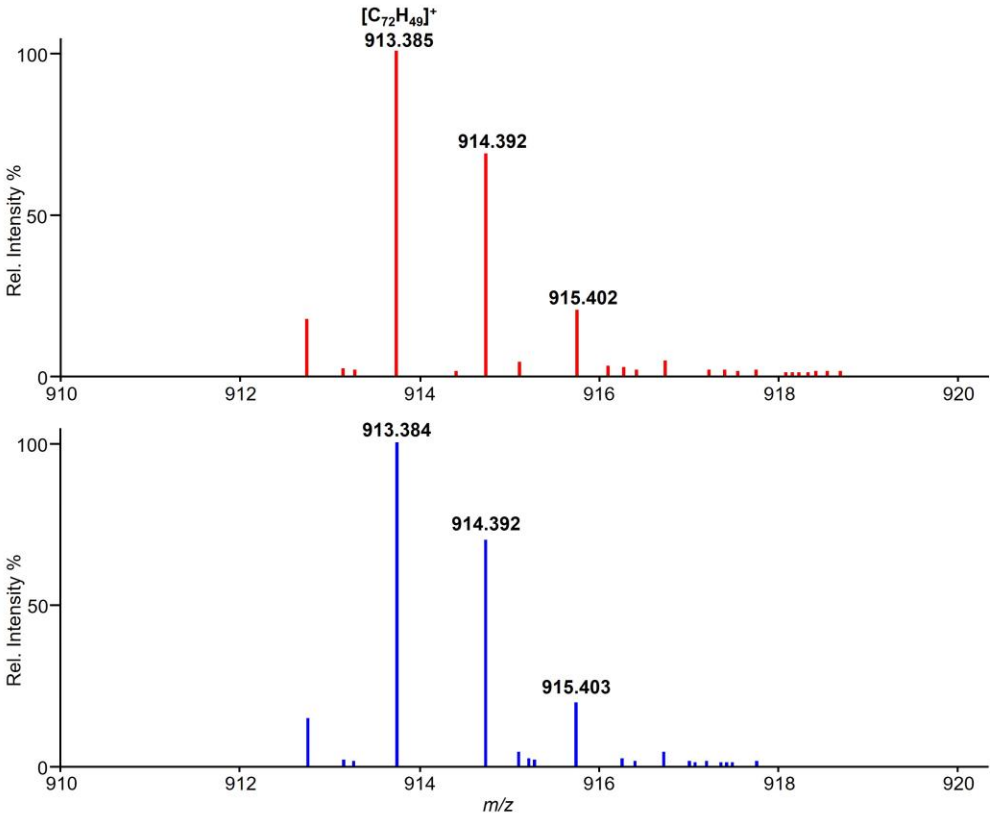

Fig. S23 DART spectra of **1** (bottom) and the quenched product of $\mathbf{1}_{TR}^{2-}$ (top).

V. Crystal Structure Solution and Refinement

Data collection of **2**·2THF was performed on a Bruker D8 VENTURE X-ray diffractometer with a PHOTON 100 CMOS detector equipped with a Cu-target, Incoatec microfocus source IμS X-ray tube (λ = 1.54178 Å) at T = 100(2) K. Data collection of **3**·3THF was performed on the same diffractometer with a Mo-target X-ray tube (λ = 0.71073 Å) at T = 100(2) K. Data reduction and integration were performed with the Bruker software package SAINT. (version 8.38A).[3] Data were corrected for absorption effects using the empirical methods as implemented in SADABS (version 2016/2).[4] The structures were solved by SHELXT (version 2018/2)[5] and refined by full-matrix least-squares procedures using the Bruker SHELXTL (version 2018/3)[6] software package through the OLEX2 graphical interface.[7] All non-hydrogen atoms (including those in disorder parts) were refined anisotropically. The H-atoms were also included at calculated positions and refined as riders, with U_{iso}(H) = 1.2 U_{eq}(C). In **2**·2THF, both [Li([2.2.2]cryptand)]$^+$ cations were found to be disordered and were modeled with two orientations. In **3**·3THF, all four 18-crown-6 molecules, seven THF molecules, and three phenyl rings of the ligands were found to be disordered and were modeled with two orientations. The geometries of the disordered parts were restrained to be similar. The anisotropic displacement parameters in the direction of the bonds were restrained to be equal with a standard uncertainty of 0.004 Å^2. They were also restrained to have the same U_{ij} components, with a standard uncertainty of 0.01 Å^2. In each unit cell of **2**·2THF, eight THF solvent molecules were found to be severely disordered and removed by the Olex2's solvent mask subroutine.[7] The total void volume was 1124.0 Å^3, equivalent to 11.6 % of the unit cell's total volume. In each unit cell of **3**·3THF, twelve THF solvent molecules were found to be severely disordered and removed by the SQUEEZE routine in PLATON (version 100419).[8] The total void volume was 2163.6 Å^3 indicated by PLATON, equivalent to 19.3 % of the unit cell's total volume. Further crystal and data collection details are listed in Table S1 and Section VII.

Table S1. Crystallographic data of **2** and **3**

Compound	**2**·2THF	**3**·3THF
Chemical formula	$C_{116}H_{136}Li_2O_{14}N_4$	$C_{124}H_{152}Na_2O_{19}$
M_r	1824.16	1992.43
Temperature (K)	100(2)	100(2)
Wavelength (Å)	1.54178	0.71073
Crystal system	Monoclinic	Monoclinic
Space group	*P*21/*c*	$P2_1$
a (Å)	31.5584(14)	13.197(3)
b (Å)	12.5876(6)	57.995(11)
c (Å)	25.8302(11)	15.630(3)
α (°)	90.00	90.00
β (°)	109.384(3)	110.696(2)
γ (°)	90.00	90.00
V (Å^3)	9679.3(8)	11191(4)
Z	4	4
F(000)	3912	4280
μ (mm^{-1})	0.640	0.085
ρ_{calcd} (g·cm^{-3})	1.252	1.054
Crystal size (mm)	0.02×0.16×0.22	0.03×0.13×0.20
Transmission factors (min/max)	0.5890/0.7528	0.6119/0.7028
Reflections collected	59724	151540
Independent reflections	16870	41044
R_{int}	0.2994	0.1396
θ range (°) for data collection	2.97–66.99	2.72–25.42
$R1[F^2 > 2\sigma(F^2)]$, $wR2(F^2)$, *S*	0.1525, 0.3945, 1.029	0.0764, 0.1802, 0.995
No. of reflections	16870	41044
No. of parameters	1623	3466
No. of restraints	4125	7996

[a]$R1 = \Sigma||F_o|-|F_c||/\Sigma|F_o|$. [b]$wR2 = [\Sigma[w(F_o^2-F_c^2)^2]/\Sigma[w(F_o^2)^2]]$.
[c]Quality-of-fit = $[\Sigma[w(F_o^2-F_c^2)^2]/(N_{obs}-N_{params})]^{½}$, based on all data.

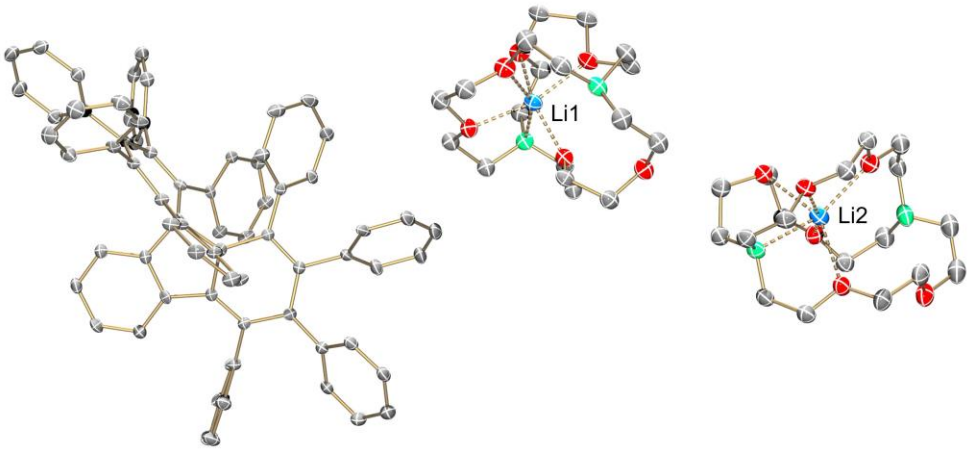

Fig. S24 ORTEP drawing of the asymmetric unit of **2** at the 40% level. H-atoms are omitted for clarity. The color scheme used: C grey, O red, N spring green, Li slate blue.

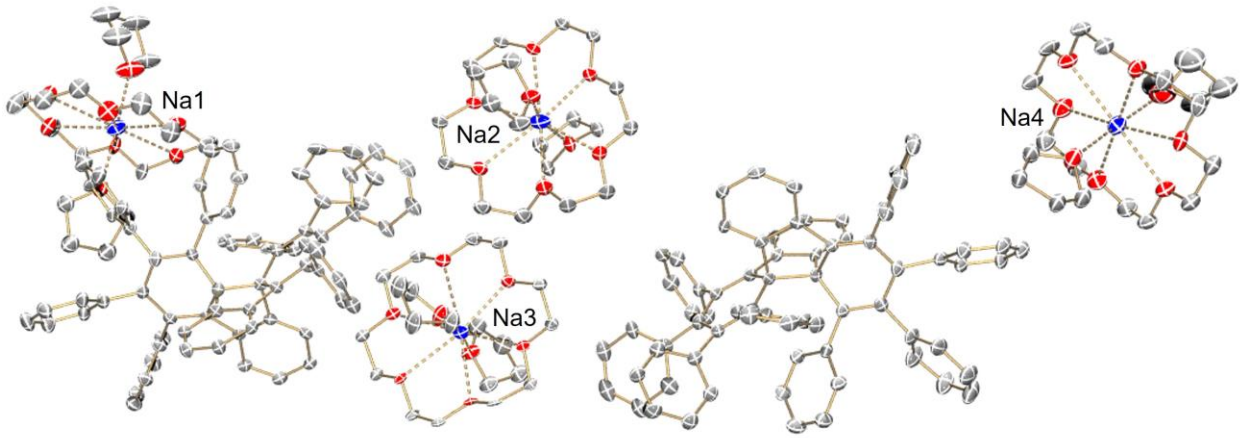

Fig. S25 ORTEP drawing of the asymmetric unit of **3** at the 40% level. H-atoms are omitted for clarity. The color scheme used: Na blue, O red, and C grey.

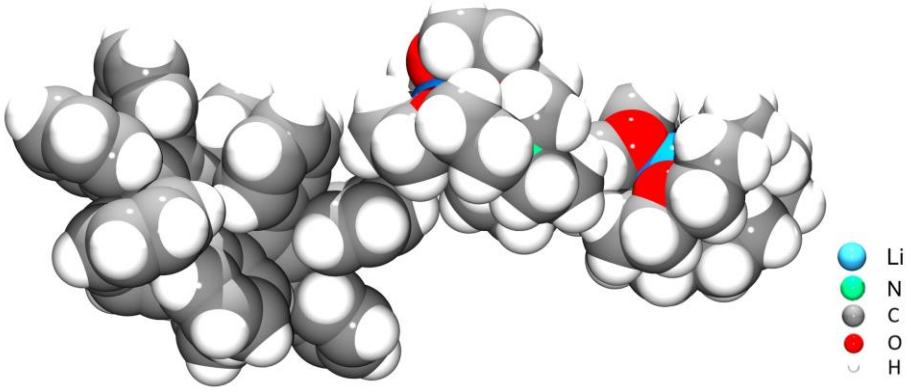

Fig. S26 Crystal structure of **2**, space-filling model.

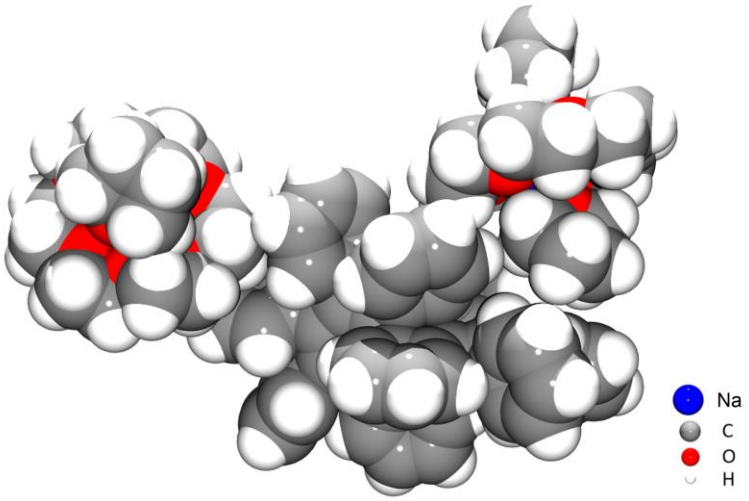

Fig. S27 Crystal structure of **3**, space-filling model.

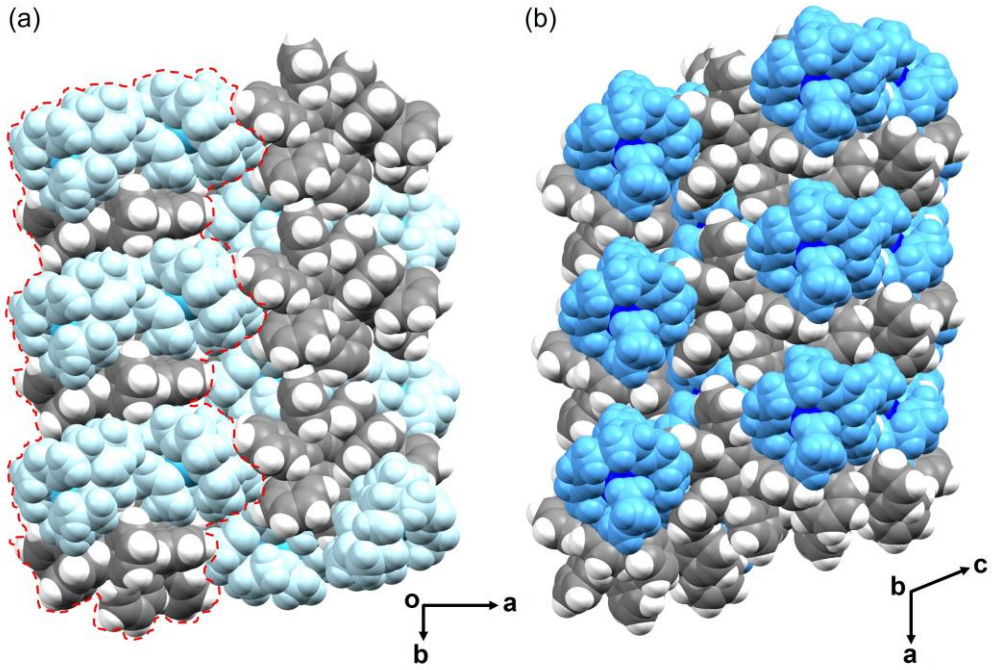

Fig. S28 Solid state packing in (a) **2** (a 1D column is highlighted) and (b) **3**, space-filling models. {Li^+([2.2.2]cryptand)} and {Na^+(18-crown-6)$(THF)_2$} moieties are shown in different shades of blue.

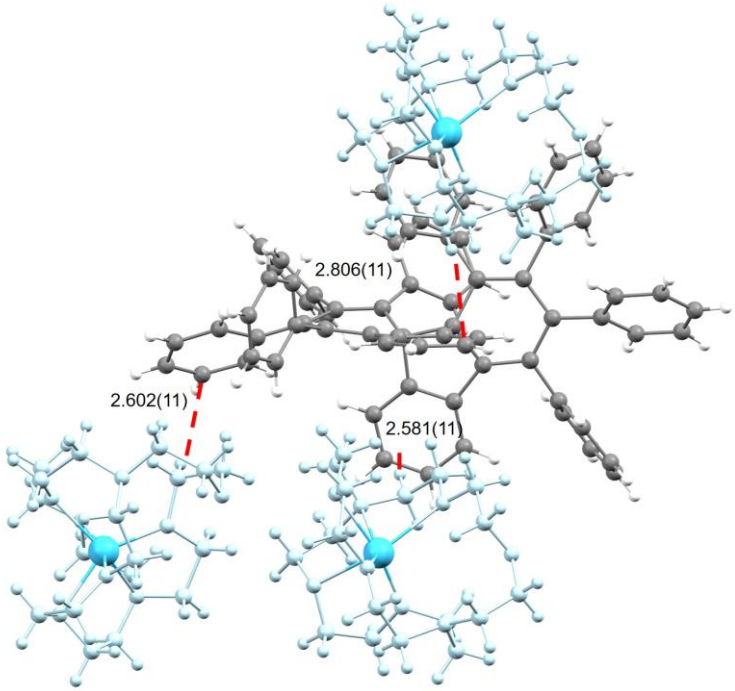

Fig. S29 C–H···π interactions in **2**, ball-and-stick model.

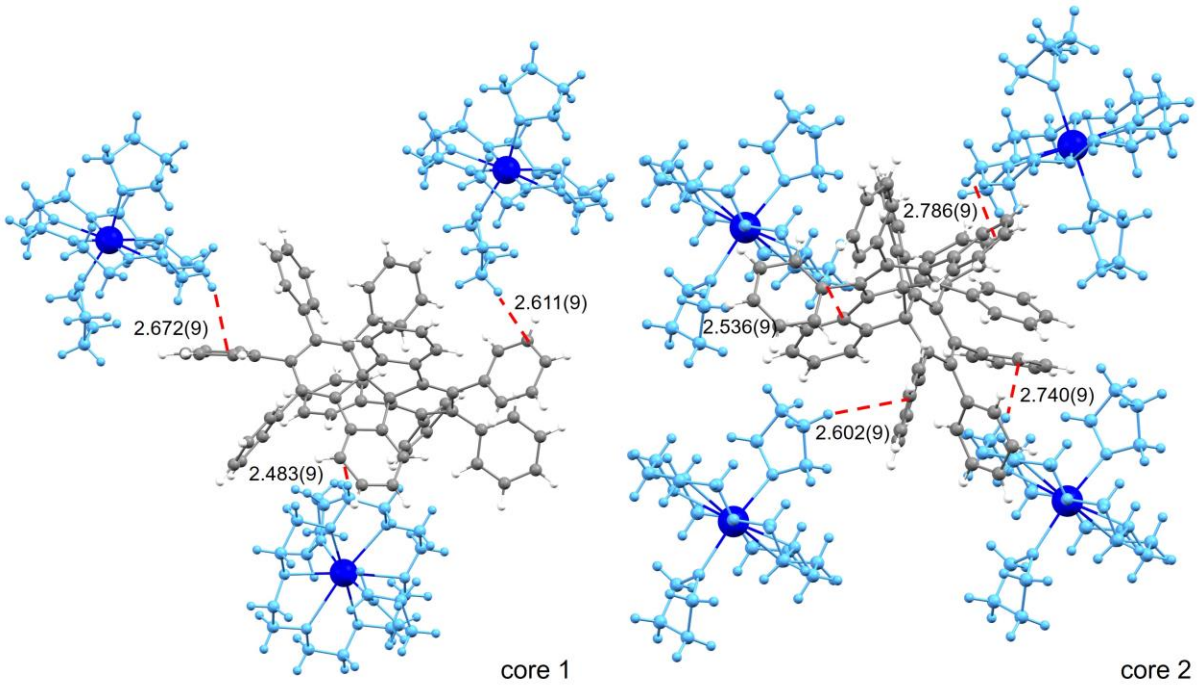

Fig. S30 C–H···π interactions in **3**, ball-and-stick model.

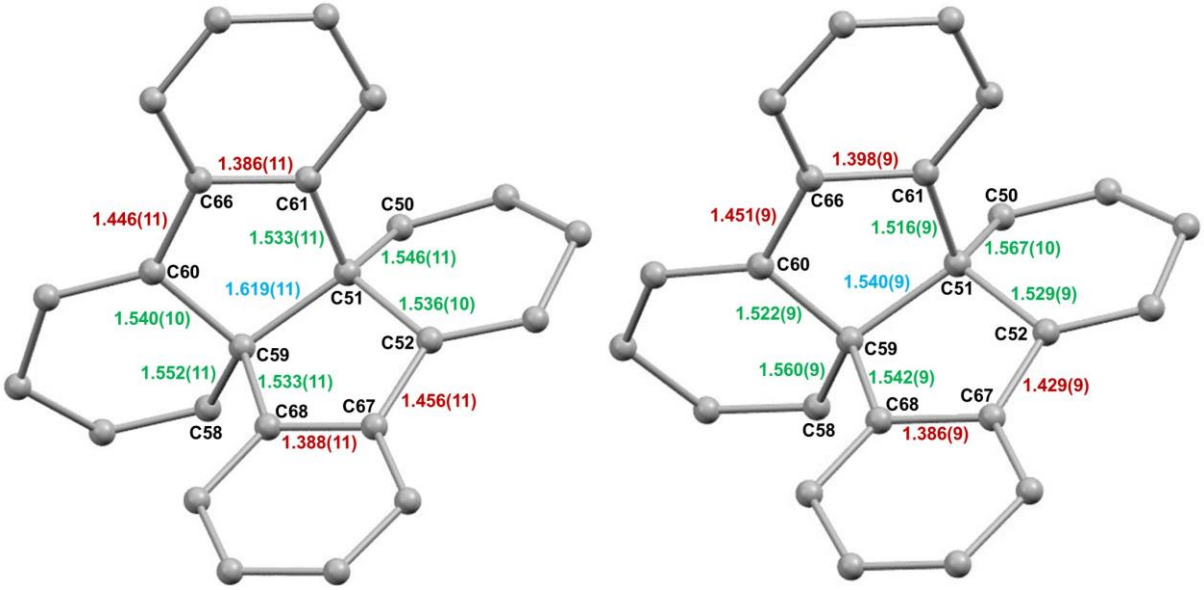

Fig. S31 Comparison of the $\mathbf{1}_{TR}^{2-}$ anions in **2** and **3**, along with the selected C–C bond distances (Å), ball-and-stick models without H-atoms. The new C–C bond is shown in blue. The elongated bonds are shown in green, whereas the shortened bonds are shown in red.

Table S2. Distances from weighted least-squares planes of selected rings (Å) in $\mathbf{1}_{TR}^{2-}$ core in **2** and **3**, along with a labeling scheme

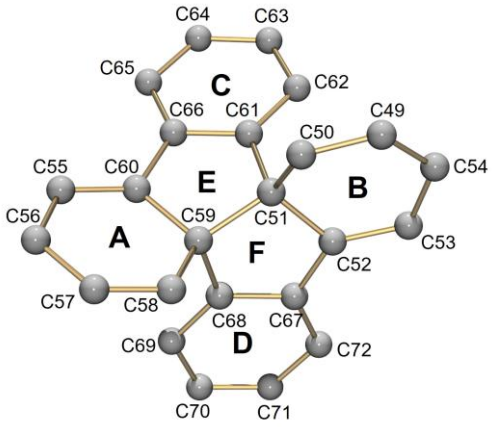

	Position	Distance		Position	Distance
Ring A	C55	0.005	Ring B	C51	–0.226
	C56	0.011		C52	0.127
	C57	0.009		C53	0.058
	C58	–0.039		C54	–0.137
	C59	0.050		C49	0.016
	C60	–0.036		C50	0.162
0.171x+0.968y+0.182z+27.640=0 (0.030)			0.929x+0.067y–0.364z+3.487=0 (0.139)		
Ring C	C61	–0.019	Ring D	C67	0.007
	C62	0.006		C68	–0.005
	C63	0.014		C69	0.001
	C64	–0.019		C70	0.001
	C65	0.004		C71	0.002
	C66	0.015		C72	–0.006
0.182x+0.821y+0.541z+29.774=0 (0.014)			0.928x–0.117y–0.354z–0.453=0 (0.004)		
Ring E	C51	–0.123	Ring F	C51	–0.145
	C59	0.153		C52	0.104
	C60	–0.128		C59	0.132
	C61	0.052		C67	–0.015
	C66	0.046		C68	–0.076
0.092x+0.782y+0.617z+29.490=0 (0.109)			0.911x–0.220y–0.349z–3.041=0 (0.105)		

	Position	Distance		Position	Distance
Ring A	C55	–0.058	Ring B	C51	0.238
	C56	0.132		C52	0.096
	C57	–0.019		C53	0.106
	C58	–0.153		C54	–0.161
	C59	0.213		C49	0.004
	C60	–0.115		C50	0.192
0.961x+0.004y–0.278z+12.887=0 (0.131)			0.095x–0.989y–0.114z–10.048=0 (0.153)		
Ring C	C61	0.018	Ring D	C67	–0.003
	C62	0.001		C68	–0.004
	C63	–0.013		C69	0.013
	C64	0.006		C70	–0.015
	C65	0.012		C71	0.008
	C66	–0.024		C72	0.001
0.878x+0.190y–0.440z+10.341=0 (0.015)			–0.093x–0.985y–0.146z–13.778=0 (0.009)		
Ring E	C51	–0.090	Ring F	C51	–0.116
	C59	0.109		C52	0.084
	C60	–0.095		C59	0.111
	C61	0.042		C67	–0.006
	C66	0.034		C68	–0.073
0.864x+0.274y–0.422z+11.367=0 (0.080)			–0.184x–0.966y–0.184z–15.931=0 (0.087)		

Table S3. Selected C–C bond distances (Å) in $\mathbf{1}_{TR}^{2-}$ in **2** and **3**

Distance	**2**	**3**	Distance	**2**	**3**
C1–C2	1.406(12)	1.428(10)	C37–C42	1.380(11)	1.376(10)
C1–C6	1.388(11)	1.410(10)	C37–C53	1.485(10)	1.492(10)
C1–C49	1.484(11)	1.424(10)	C38–C39	1.363(12)	1.354(10)
C2–C3	1.390(12)	1.337(10)	C39–C40	1.380(13)	1.353(11)
C3–C4	1.371(13)	1.375(12)	C40–C41	1.368(13)	1.402(11)
C4–C5	1.378(14)	1.347(12)	C41–C42	1.380(12)	1.394(11)
C5–C6	1.384(12)	1.397(11)	C43–C44	1.408(11)	1.404(10)
C7–C8	1.394(11)	1.444(10)	C43–C48	1.423(12)	1.404(10)
C7–C12	1.390(11)	1.369(10)	C43–C54	1.462(11)	1.464(10)
C7–C50	1.457(11)	1.469(10)	C44–C45	1.391(12)	1.369(11)
C8–C9	1.391(11)	1.355(10)	C45–C46	1.402(13)	1.382(12)
C9–C10	1.388(13)	1.379(10)	C46–C47	1.358(12)	1.375(12)
C10–C11	1.392(14)	1.395(11)	C47–C48	1.378(12)	1.397(11)
C11–C12	1.407(12)	1.368(10)	C49–C50	1.381(11)	1.398(10)
C13–C14	1.385(12)	1.336(10)	C49–C54	1.458(11)	1.461(10)
C13–C18	1.385(12)	1.407(10)	C50–C51	1.546(11)	1.567(10)
C13–C55	1.500(11)	1.468(9)	C51–C52	1.536(10)	1.529(9)
C14–C15	1.392(12)	1.392(10)	C51–C59	1.619(11)	1.540(9)
C15–C16	1.343(13)	1.369(11)	C51–C61	1.533(11)	1.516(9)
C16–C17	1.349(14)	1.375(11)	C52–C53	1.351(11)	1.386(10)
C17–C18	1.386(12)	1.386(9)	C52–C67	1.456(11)	1.429(9)
C19–C20	1.387(12)	1.388(15)	C53–C54	1.448(11)	1.437(10)
C19–C24	1.386(11)	1.391(15)	C55–C56	1.440(11)	1.454(9)
C19–C56	1.479(11)	1.491(15)	C55–C60	1.384(11)	1.398(9)
C20–C21	1.392(12)	1.388(14)	C56–C57	1.430(11)	1.427(9)
C21–C22	1.359(13)	1.371(16)	C57–C58	1.359(11)	1.345(9)
C22–C23	1.379(14)	1.359(16)	C58–C59	1.552(11)	1.560(9)
C23–C24	1.398(12)	1.400(15)	C59–C60	1.540(10)	1.522(9)
C25–C26	1.397(11)	1.411(11)	C59–C68	1.533(11)	1.542(9)
C25–C30	1.385(11)	1.387(11)	C60–C66	1.446(11)	1.451(9)
C25–C57	1.524(11)	1.503(10)	C61–C62	1.395(11)	1.405(9)
C26–C27	1.372(12)	1.386(10)	C61–C66	1.386(11)	1.398(9)

C27–C28	1.375(13)	1.364(12)	C62–C63	1.403(11)	1.403(9)
C28–C29	1.375(13)	1.357(12)	C63–C64	1.377(12)	1.349(10)
C29–C30	1.391(12)	1.416(11)	C64–C65	1.380(11)	1.402(10)
C31–C32	1.403(10)	1.408(9)	C65–C66	1.413(11)	1.417(9)
C31–C36	1.379(10)	1.387(9)	C67–C68	1.388(11)	1.386(9)
C31–C58	1.472(10)	1.491(9)	C67–C72	1.399(11)	1.424(9)
C32–C33	1.412(11)	1.376(9)	C68–C69	1.387(11)	1.386(10)
C33–C34	1.388(11)	1.344(10)	C69–C70	1.370(11)	1.403(10)
C34–C35	1.379(12)	1.395(10)	C70–C71	1.383(12)	1.361(10)
C35–C36	1.371(11)	1.403(9)	C71–C72	1.359(12)	1.377(10)
C37–C38	1.389(11)	1.361(10)			

VI. Quantum-Chemical Calculations

Computational Details

All calculations were performed using the program package Turbomole (version 7.3),[9] and were carried out on the DFT level (within Kohn-Sham theory) applying the B3LYP exchange-correlation functional[10] and the def2-TZVP basis set family[11] if not stated otherwise (in the following, the prefix def2- will be omitted). Throughout, the multipole accelerated RI method[12-14] was used to calculate the Coulomb part of the electronic energy, and Grimme's D3 dispersion correction[15] was adopted (w/o damping).

Solvent effects are captured within the conductor-like screening model (COSMO)[16] with the dielectric constant $\epsilon = 7.6$ mimicking THF. In case of neutral molecules, we used the usual COSMO screening factor $f = \frac{\epsilon-1}{\epsilon+\frac{1}{2}}$, whereas for charged molecules final energies were evaluated with $f = \frac{\epsilon-1}{\epsilon}$, as it has been shown that this is more accurate for ions.[17] In any case, energies were corrected for the so-called outlying-charge error as described in Ref. [18]. We use the shorthand notation COSMO-B3LYP/TZVP to denote this level of theory.

After geometry optimization, vibrational harmonic frequencies were obtained by numerical differentiation using the module NumForce from the Turbomole suite. We verified that minimum structures do not exhibit any imaginary frequencies and that transition states possess exactly one imaginary frequency. Finally, thermal corrections to the free enthalpy G at standard conditions (T = 298K, p = 1bar) are computed using a modified harmonic-oscillator approximation that interpolates the entropic contributions of low-frequency vibrations below 300 cm^{-1} between a free rotator model and the (usual) harmonic oscillator model, see Ref. [19] for details. This methodology leads to a more balanced description of the entropy contributions from these low-frequency vibrations (within the commonly adopted harmonic approximation the entropy contributions of low-frequency vibrations are notoriously overestimated).

The reaction energy ($\Delta H°$, $\Delta G°$) of the reduction

2 Li(solid) + **1** + 2 [2.2.2]cryptand $\rightarrow$ $\mathbf{1}^{2-}$ + 2 {Li^+([2.2.2]cryptand)}

was calculated by partitioning the overall reaction according to

(1) 2 Li(solid) $\rightarrow$ Li_2(gas phase)

(2) Li_2(gas phase) + **1** + 2 [2.2.2]cryptand $\rightarrow$ $\mathbf{1}^{2-}$ + 2 {Li^+([2.2.2]cryptand)}

and using the experimental vaporization energies of solid lithium[20] for reaction (1):

$\Delta H° = +51.6$ kcal/mol, $\Delta G° = +41.7$ kcal/mol.

Li_2(gas phase) was treated as a perfect gas.

Structures and Charge Distributions:

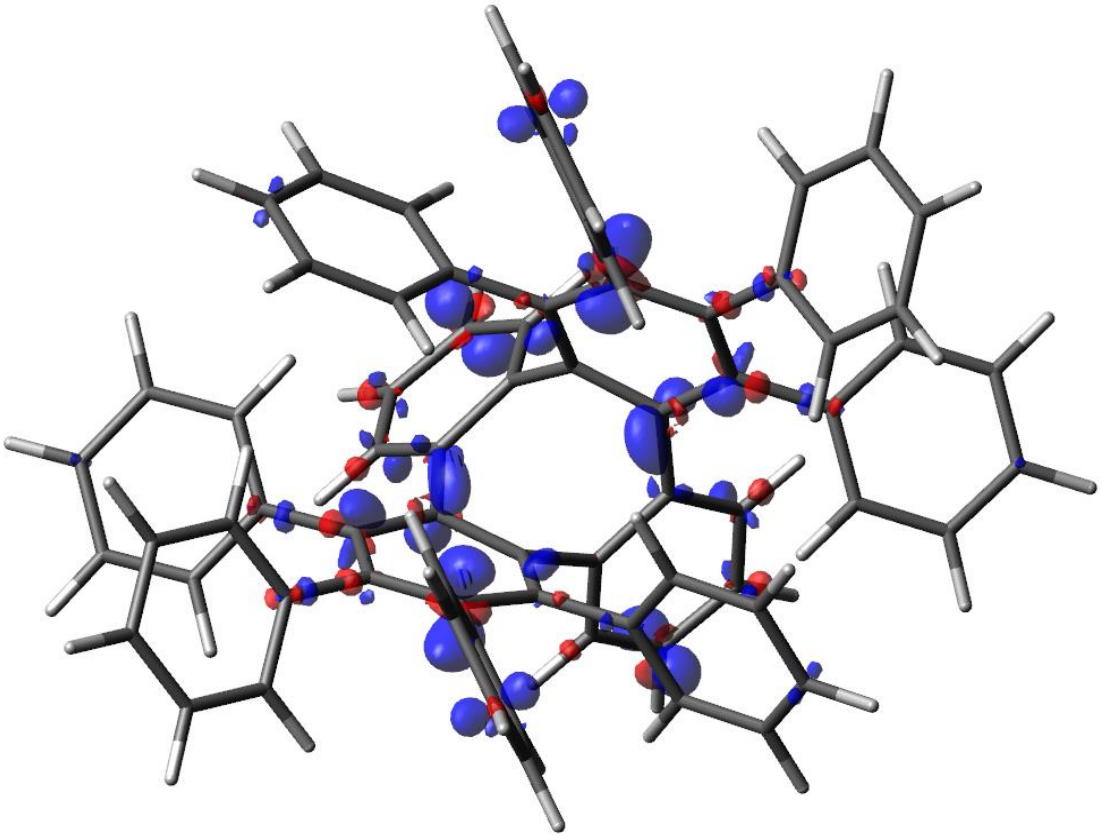

Fig. S32 Optimized structure and differential charge distribution of $\mathbf{1}^{2-}$ (with respect to neutral **1** at the same geometry). Blue: Increase of electron density, red: decrease of electron density. Iso-surfaces plotted at 0.004 e/Bohr^{-3}.

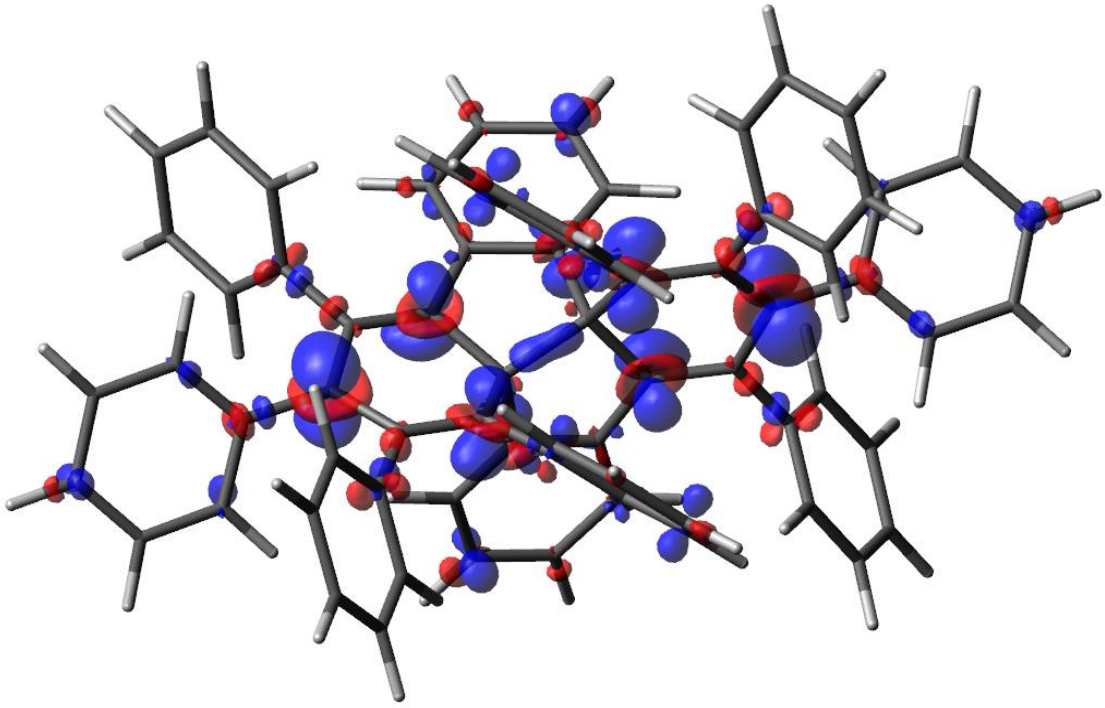

Fig. S33 Optimized structure and differential charge distribution of $\mathbf{1}_{TR}^{2-}$ (with respect to neutral $\mathbf{1}_{TR}$ at the same geometry). Blue: Increase of electron density, red: decrease of electron density. Iso-surfaces plotted at 0.004 e/Bohr^{-3}.

Computed Energies:

Computed SCF energies and zero-point vibrational energies (ZPVE) in Hartree on the COSMO-B3LYP/TZVP level of theory (except Li_2 (gas phase) which was calculated without COSMO).

	1	**1**$^{-}$	**1**$_{TR}^{-}$	**1**$^{2-}$	**1**$_{TR}^{2-}$
E(SCF)	-2771.997107	-2772.052488	-2772.013941	-2772.087051	-2772.091268
ZPVE	0.966777	0.978733	0.978452	0.973850	0.975950
	1a	**1a**$^{-}$	**1a**$_{TR}^{-}$	**1a**$^{2-}$	**1a**$_{TR}^{2-}$
E(SCF)	-923.998514	-924.046643	-923.998322	-924.073195	-924.078869
ZPVE	0.321915	0.316758	0.315401	0.314002	0.313007
	[2.2.2]cryptand	Li^{+}([2.2.2]cryptand)	Li_2 (gas ph.)	[**1a**$^{2-}$]$^{\neq}$	
E(SCF)	-1268.143167	-1275.645829	-14.997218	-924.050752	
ZPVE	0.553779	0.559651	0.000755	0.311671	

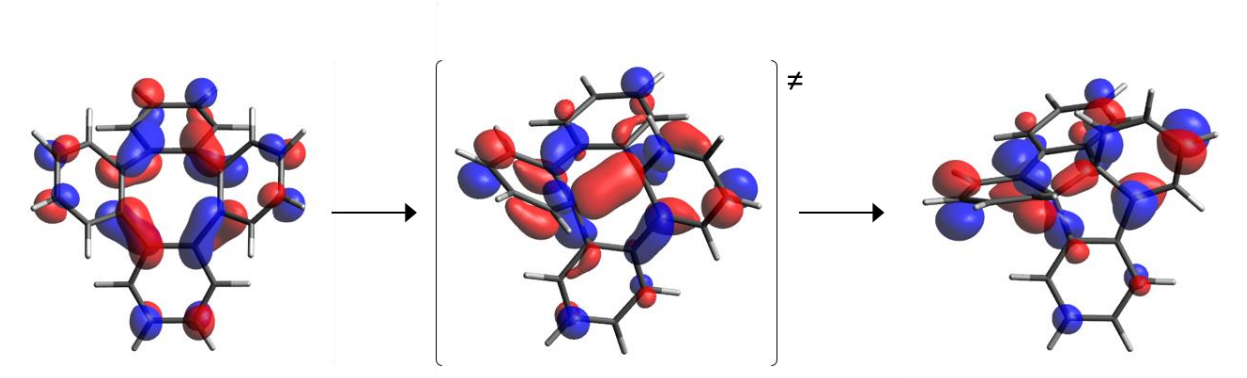

Fig. S34 HOMO upon transformation of **1a**$^{2-}$ (= **1**$^{2-}$ without phenyl substituents). Iso-surfaces plotted at 0.04 Bohr$^{-3/2}$.

VII. Comment on Crystallographic Data Quality

Figs. 35-38 show that the effective resolution of **2** and **3** does not reach the minimum required resolution of 0.84 Å due to weak diffraction of the corresponding single crystals. On the in-house single crystal X-ray diffractometer, the exposure time was set as 60 seconds, but the diffraction was still not strong enough. Longer exposure times were also tried but the background noise has dramatically increased with the prolonged exposure times, which as a result, did not lead to better quality data. It should be noted that the reported data of **2** and **3** are not the only data sets that were ever collected. Before publication, multiple crystals of **2** and **3** have been checked from different reactions, different sample batches, different crystal growth methods, and using different wavelengths for data collection (Mo and Cu radiation for our in-house single crystal X-ray diffraction instrument, and synchrotron X-ray diffraction facilities in Argonne National Laboratory). However, none of them yield stronger diffraction data than the data presented. This could stem from two factors: 1) The unit cells of both **2** and **3** are large (close to 10,000 $Å^3$), which typically results in a less orderly packing.[21-24] 2) Both **2** and **3** contain severely disordered solvent molecules, which also lead to loose packing and as a result, weak diffraction.[25] Due to these limiting factors, it was impossible to obtain stronger data even though very powerful X-ray source and optimal settings were employed for data collections of **2** and **3**.

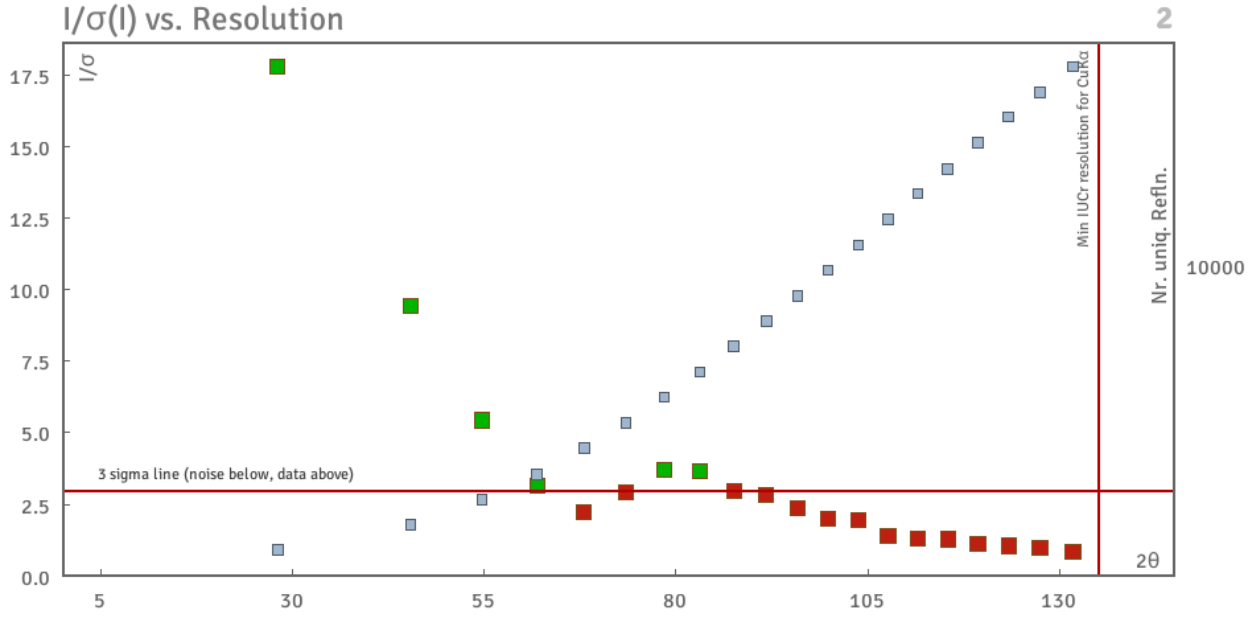

Fig. S35 Plot of $I/\sigma(I)$ *vs.* resolution for crystal data of **2**.

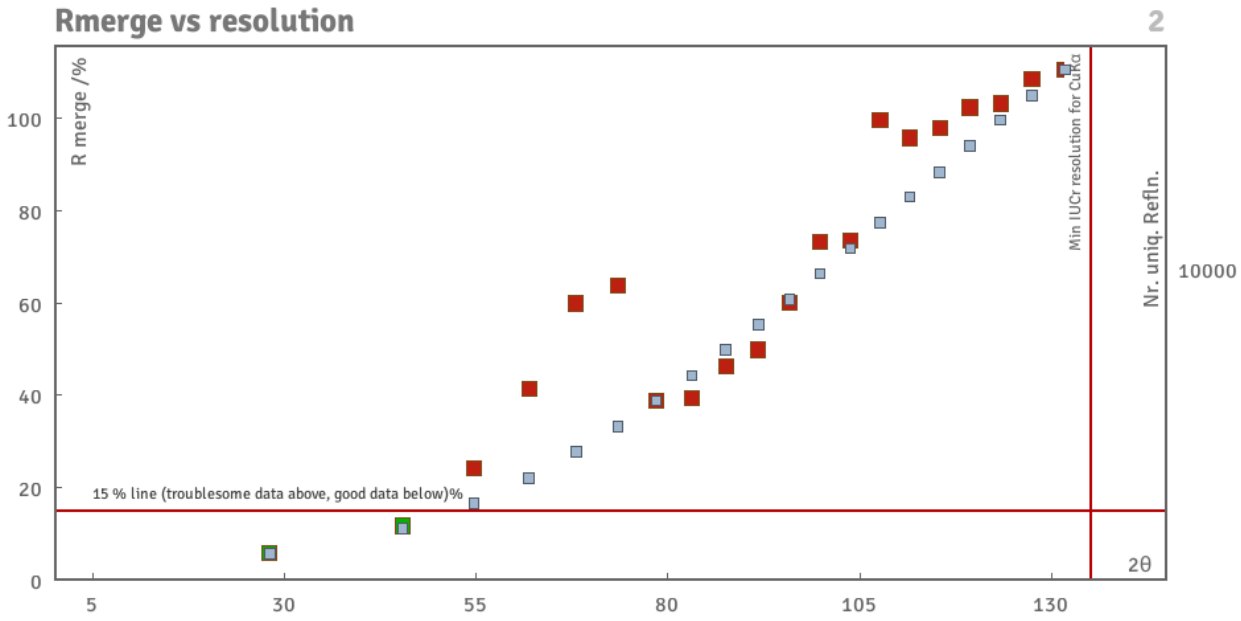

Fig. S36 Plot of R_{merge} *vs.* resolution for crystal data of **2**.

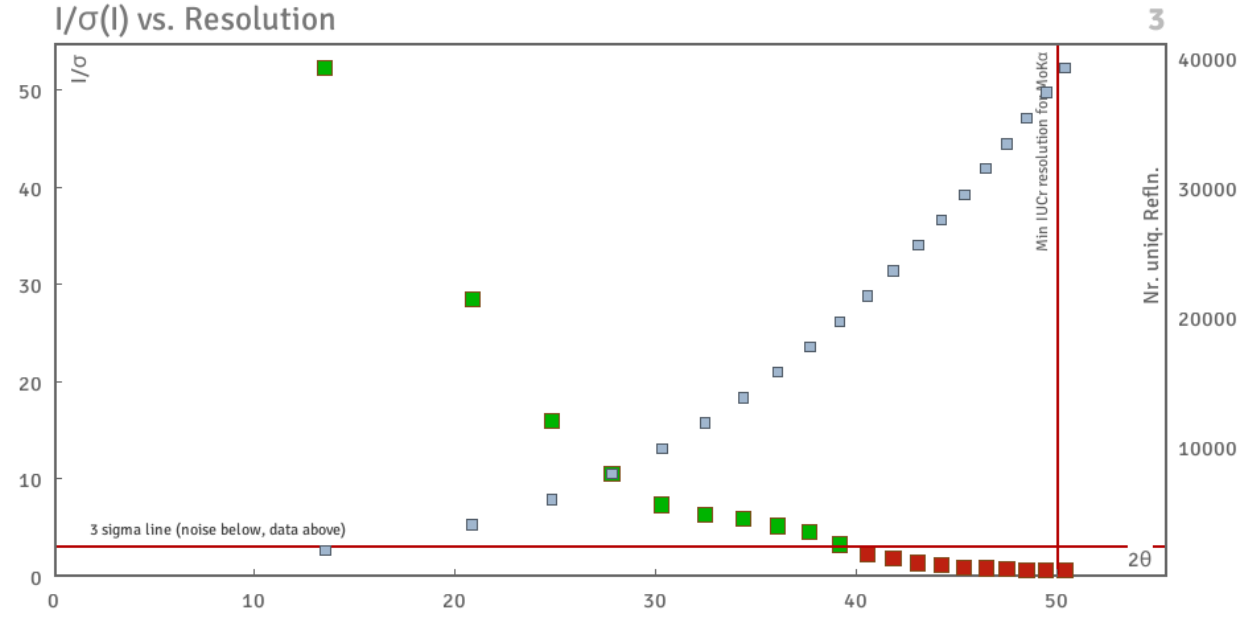

Fig. S37 Plot of $I/\sigma(I)$ *vs.* resolution for crystal data of **3**.

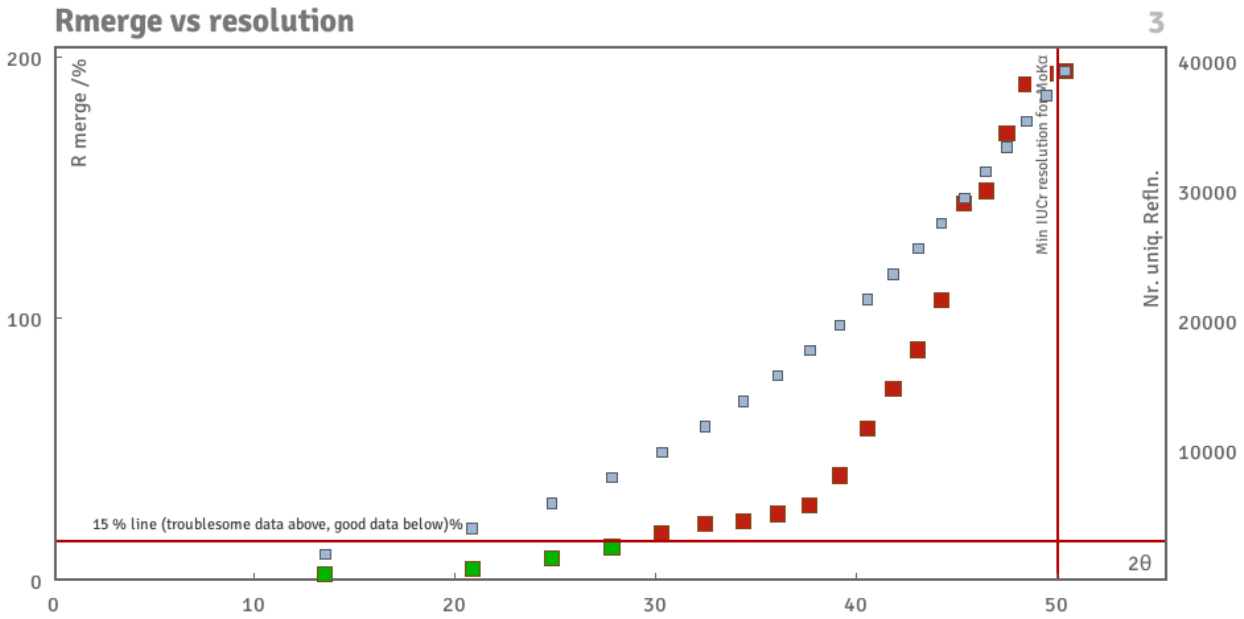

Fig. S38 Plot of R_{merge} *vs.* resolution for crystal data of **3**.

VIII. References

[1] N. V. Kozhemyakina, J. Nuss and M. Jansen, *Z. Anorg. Allg. Chem.*, 2009, **635**, 1355-1361.

[2] Z. Zhou, Y. Zhu, Z. Wei, J. Bergner, C. Neiß, S. Doloczki, A. Görling, M. Kivala and M. A. Petrukhina, *Angew. Chem. Int. Ed.*, 2020, **60**, 3510-3514.

[3] SAINT; part of Bruker APEX3 software package (version 2016.9-0): Bruker AXS, 2016.

[4] SADABS; part of Bruker APEX3 software package (version 2016.9-0): Bruker AXS, 2016.

[5] G. M. Sheldrick, *Acta Crystallogr.*, 2015, **A71**, 3-8.

[6] G. M. Sheldrick, *Acta Crystallogr.*, 2015, **C71**, 3-8.

[7] O. V. Dolomanov, L. J. Bourhis, R. J. Gildea, J. A. K. Howard and H. Puschmann, *J. Appl. Crystallogr.*, 2009, **42**, 339-341.

[8] A. L. Spek, *Acta Crystallogr. C*, 2015, **71**, 9-18.

[9] TURBOMOLE V7.3 2018, a development of University of Karlsruhe and Forschungszentrum Karlsruhe GmbH, 1989-2007, TURBOMOLE GmbH, since 2007; available from *http://www.turbomole.com*.

[10] A. D. Becke, *J. Chem. Phys.*, 1993, **98**, 5648-5652.

[11] F. Weigend and R. Ahlrichs, *Phys. Chem. Chem. Phys.*, 2005, **7**, 3297-3305.

[12] K. Eichkorn, O. Treutler, H. Öhm, M. Häser and R. Ahlrichs, *Chem. Phys. Lett.*, 1995, **242**, 652-660.

[13] M. Sierka, A. Hogekamp and R. Ahlrichs, *J. Chem. Phys.*, 2003, **118**, 9136-9148.

[14] F. Weigend, *Phys. Chem. Chem. Phys.*, 2006, **8**, 1057-1065.

[15] S. Grimme, J. Antony, S. Ehrlich and H. Krieg, *J. Chem. Phys.*, 2010, **132**, 154104.

[16] A. Klamt and G. Schüürmann, *J. Chem. Soc., Perkin Trans., 2* 1993, 799-805.

[17] A. Klamt, C. Moya and J. Palomar, *J. Chem. Theo. Comp.*, 2015, **11**, 4220-4225.

[18] A. Klamt and V. Jonas, *J. Chem. Phys.*,1996, **105**, 9972-9981.

[19] S. Grimme, *Chem. Eur. J.*, 2012, **18**, 9955-9964.

[20] *CRC Handbook of Chemistry and Physics* 2017, Section 5: Standard Thermodynamic Properties of Chemical Substances.

[21] M. Coletta, T. G. Tziotzi, M. Gray, G. S. Nichol, M. K. Singh, C. J. Milios, E. K. Brechin, *Chem. Commun.* 2021, **57**, 4122-4125.

[22] B. L. Ouay, H. Yoshino, K. Sasaki, Y. Ohtsubo, R. Ohtani, M. Ohba, *Chem. Commun.* 2021, **57**, 5187-5190.

[23] A. Wong, A. Chakraborty, D. Bawari, G. Wu, R. Dobrovetsky, G. Ménard, *Chem. Commun.* 2021, **57**, 6903-6906.

[24] M. S. Smyth, J. H. J. Martin, *Mol. Pathol.* 2000, **53**, 8-14.

[25] B. Heras, J. L Martin, *Acta Cryst.* 2005, **D61**, 1173-1180.